CORROSION KINETICS OF AUSTENITIC STAINLESS STEEL UNDER WATER NORMAL OPERATION PWR CONDITION

V.S.P. SILVA

Amazônia Azul Tecnologias de Defesa S.A. - AMAZUL São Paulo, Brazil

Email: vanessa.sanches@marinha.mil.br

F. CAMARGO

Amazônia Azul Tecnologias de Defesa S.A. - AMAZUL São Paulo, Brazil.

INTRODUCTION: There is a growing global interest in enhancing the operational reliability, economic performance, and safety of nuclear power plants, particularly in the aftermath of the Fukushima Daiichi incident. The development of advanced materials has driven the search for accident tolerant fuels (ATFs), which offer improved performance under normal, transient, and accident conditions.

As part of the evaluation of potential ATF materials, long-term corrosion tests were conducted using a niobium-stabilized austenitic stainless steel (Nb-ASS). Due to the limited available data on the corrosion behavior of this alloy under such conditions, two separate tests were performed. The first involved both tube and plate coupons, while the second focused on plates, in order to evaluate the possible influence of the autoclave used during exposure. All samples were exposed to ultrapure, deoxygenated water at 360 °C and 20 MPa for approximately 84 days, in cycles of about 21 days, with the objective of modeling the oxidation rate.

The oxidation behavior typically observed in stainless steels under these conditions is characterized by the formation of two distinct oxide layers on the surface: an outer magnetite layer and an inner chromium-rich (chromite) spinel layer. X-ray diffraction (XRD) analysis confirmed the presence of these phases on samples tested. Based on this, a model assuming equal proportions of magnetite and chromite was adopted to estimate the oxide bilayer thickness. The paper presents the methodology used to estimate oxide layer thickness from mass gain data and compares the results with values reported in the literature for Zr-, Fe- and Ni-base alloys.

Moreover, assuming a solid-state diffusion mechanism and parabolic oxidation kinetics, both the weight gain kinetic constant and the corresponding oxide growth rate were determined. This approach not only confirms the high oxidation resistance of the tested ATF candidate under normal operating conditions — compared to conventional Zr-base alloys — but also demonstrates its similarity to commonly used stainless steels, such as AISI 304 SS, whose oxidation behavior is well established in reactor environments.

1. MATERIALS AND METHODS

Two rounds of long-term corrosion testing in ultrapure and deoxygenated water (DO₂ < 0.05 ppm / DH₂ < 5 ppb) at 360 °C and 20 MPa were performed. The first one used four sets of triplicate specimens, in both tube and plate geometries during 84.5 days of exposure inside autoclaves connected to a recirculating water loop. The second one repeated the first round using only plates specimens with twice as many samples for 84 days.

The corrosion tests were carried out using two autoclaves integrated into a recirculating loop system equipped with online monitoring of temperature, pressure, electrical conductivity, dissolved oxygen (DO₂), and dissolved hydrogen (DH₂) operating in dynamic mode (11/min). The ultra-pure water was treated with nitrogen (99.999 %) and ion exchanges resins passed through autoclave 1 (AC1) and then to autoclave 2 (AC2) returning to treated station. XRD with Bragg-Brentano geometry and cupper radiation were made on plates coupons to identify the oxide phases formed onto Nb-ASS surface.

2. RESUSTS AND DISCUSSION

2.1. Weight Gain

The surface mass gain (Wg) results for all the samples tested were joined accordingly the test with some groups. In the first round it was analysed the differences between the type of specimens tested (tube or plate), and in the second one the groups were separated by autoclave as TABLE 1shows.

TABLE 1	WEIGHT	GAIN RESULTS	AND OXIDE	THICKNESS C.	ALCULATION
	, WEIGHT	G/III I ILBULIS	M M M M M M M M M M		ILCOLITION.

Test	Coupon	Exposure time (Autoclave)	Weight gain (mg/dm²)	Oxide thickness estimated (µm)
1 —	Plates	21.0 d (both)	1.64 ± 0.51	0.117 ± 0.037
		63.5 d (both)	2.81 ± 0.78	0.201 ± 0.056
		84.5 d (both)	3.60 ± 0.44	0.257 ± 0.033
	Tubes	21.0 d (both)	3.22 ± 0.15	0.230 ± 0.014
		63.5 d (both)	4.06 ± 0.48	0.290 ± 0.036
		84.5 d (both)	5.00 ± 0.39	0.357 ± 0.031
2	Plates	34 d (AC1)	0.98 ± 0.36	0.070 ± 0.026
		42 d (AC1)	1.02 ± 0.37	0.073 ± 0.027
		63 d (AC1)	1.09 ± 0.51	0.078 ± 0.037
		84 d (AC1)	1.56 ± 0.56	0.111 ± 0.040
		21 d (AC2)	1.38 ± 0.37	0.099 ± 0.027
		34 d (AC2)	3.6 ± 0.49	0.257 ± 0.036
		42 d (AC2)	3.72 ± 0.47	0.266 ± 0.035
		63 d (AC2)	4.26 ± 0.47	0.304 ± 0.035

Based on solid state diffusion model proposed by Robertson [1] the general corrosion rate of a stainless steel (SS) can be considered parabolic. Performing a weighted linear fit, taking into account the uncertainties in the squared mass gain measurements, it was possible to determine the experimental parabolic weight gain kinetic constant (k_p^{Wg}) in $(mg/dm^2)^2/d$, as shown in FIG. 1a, where the slope values correspond to k_p^{Wg} for each specimen type tested in the first round performed at this study.

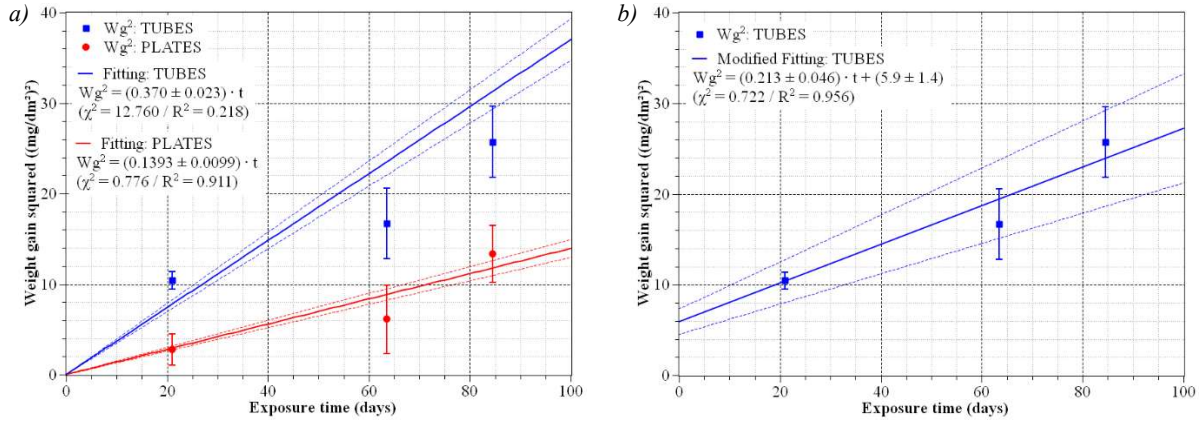


FIG. 1 Fittings used to obtain parabolic weight gain kinetic constant (slope) in $(mg/dm^2)^2/d$ for a) plates and tubes specimens tested on round 1 according to [1] and b) tubes according to [2].

According to Pieraggi [2], the parabolic law $(Wg^2 = k_p^{Wg} \cdot t)$ does not accurately model the initial stages of corrosion, thus by modeling the mass gain data as done here the resulting k_p^{Wg} value tends to be overestimated. Therefore, a better estimate of the oxidation kinetics of Nb-ASS tubes coupons can be obtained using a complete first-degree function, rather than the simplified model. It was done at FIG. *I*b, that presents the results of a modified parabolic fit for the tube samples. In this case, considering the uncertainties, the model provides a better fit when the initial stages of corrosion are excluded.

Similar consideration was made for the second test and the corrosion rate found for samples treated into the different autoclaves were distinct. Samples tested on AC1 presents smaller kinetic constant ($k_{p,\,AC1}^{Wg} = 0.0424 \pm 0.0038 (mg/dm^2)^2/d$) when compared to results from AC2 where ($k_{p,\,AC2}^{Wg} = 0.231 \pm 0.015 \ (mg/dm^2)^2/d$). However, the second test proved the repeatability of the long corrosion test performed, since kinetic parabolic constant found, $k_p^{Wg} = 0.1367 \pm 0.0077 \ (mg/dm^2)^2/d$, was the same of the first one for plates $0.1393 \pm 0.0099 \ (mg/dm^2)^2/d$ (see slope for plates at FIG. 1a).

The paper results were plotted against the compilated presented at Pessl report [3] as showed at FIG. 2 and proved closely agreement to results from 300-series stainless steel.

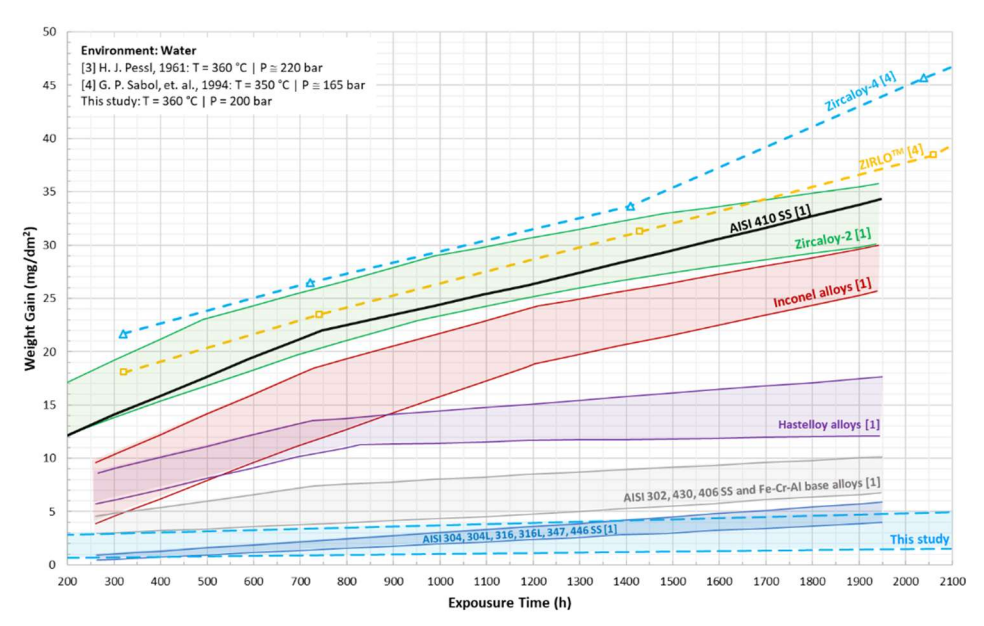


FIG. 2 Comparison between experimental results and literature data, adapted from H.J. Pessl [3]

2.2. XRD

XRD results showed that by using a conventional Bragg-Brentano geometry, even to identify such a thinner layer, was possible to observe the presence of spinel structure (M₃O₄) or magnetite (Fe₃O₄) for all plate coupons tested, as expected based on literature [1, 5-6]. Besides the face-centered-cell (FCC) structure, characteristic of austenitic iron phase, it was also observed the presence of iron body-centered-cell (BCC) phase. However, an analysis from a plate coupon not oxidized shown that BCC phase was previous present on specimen surface, probably due to cold work induced martensite.

2.3. Thickness from Weight Gain

Considering oxidation on both sides of a tube, and using the approximation that the surface area of the tube's inner wall is approximately equal to that of the outer wall, $(A_{int} \approx A_{ext} \equiv A)$ the total volume of base metal reacted during oxidation would be $V_{metal} = A \cdot t_{metal}^{total}$, where t_{metal}^{total} is the total thickness of metal reacted. Considering that all weight gain measured refers to the mass of oxygen reacting stoichiometric to the base metal (M) to form oxide, and that none mass loss due to spallation occurs

during corrosion test (Wg = $m_{O_2}/2A$) the generic reaction: Y metal + X/2 $O_2 \rightarrow M_y O_x$ leads to the following relationship:

$$m_{\text{metal}} = \frac{1}{f_{O_2/\text{oxide}}} \cdot m_{O_2} \tag{1}$$

where $f_{O_2/oxide} \equiv M_{XO}/M_{Y metal}$.

From density definition, equation 1 can be rewritten to $t_{metal}^{total} = 2Wg/f_{O_2/oxide} \cdot \rho_{metal}$. However, if instead of consider the mass of metal consumed during oxidation, the mass of oxide produced during the long-term test was used, an analogous equation can be found replacing the index of metal to oxide. By doing this and adjusting the units, it is possible to determine the conversion constant between the thickness of the oxide formed on one side and the total mass gain measured experimentally.

$$t_{\text{oxide}}[\mu m] = k_{\text{conversion}} \cdot Wg[mg/dm^2]$$
 (2)

$$k_{conversion} = \frac{1}{10 \cdot f_{0_2/oxide} \cdot \rho_{oxide}[g/cm^3]}$$
(3)

where $f_{O_2/oxide}$ is the fraction of the molar mass of oxygen present in the formed oxide relative to the molar mass of the oxide, and ρ_{oxide} is the density of the formed oxide.

Considering a bilayer formed of equal parts of magnetite and chromite (spinel), without any addition of porosity correction, $k_{conversion}$ were estimated from Equation 3 for Nb-ASS and was found to be $0.0714 \pm 0.0027~\mu m \cdot dm^2/mg$. This value and Equation 2 was used to estimate the oxide thickness showed at TABLE 1. Using this constant and the oxidation rate found for oxide thickness, a projected thickness range was calculated for the Nb-ASS assuming 150 days of exposure test, in order to compare with the data presented by Pessl [3] and to validate the method used here. The results showed that within the calculated range $(0.12-0.55~\mu m)$ were found several 300-series stainless steels, including AISI 304, 316, and 347 SS.

3. CONCLUSIONS

The niobium-stabilized austenitic SS studied by the paper exhibited notable oxidation resistance in water under normal operation PWR condition, characterized by parabolic kinetics and the formation of a bilayer oxide structure comprising magnetite and spinel phases, as confirmed by XRD analysis. The oxide layer thickness was reliably estimated from mass gain data using a derived conversion constant. These results support its potential as an ATF cladding material, showing corrosion behavior comparable to that of 300-series stainless steels and superior to conventional Zr-base alloys under normal operating conditions. Furthermore, the consistency observed across test campaigns reinforces the reliability and repeatability of the applied methodology.

REFERENCES

- [1] ROBERTSON, J., The Mechanism of High Temperature Aqueous Corrosion of Stainless Steels, Corrosion Science **32** 4 (1991) 443–465, https://doi.org/10.1016/0010-938X(91)90125-9.
- [2] PIERRAGI, B., Calculations of Parabolic Reaction Rate Constants, Oxidation of Metals 27 (1987) 177–185, https://doi.org/10.1007/BF00667057.
- [3] PESSL, H. J., Evaluation of Iron- and Nickel-base alloys for medium and high temperature reactor applications. Part I. HW-67715, Washington, 1961.
- [4] SABOL, G. R., COMSTOCK, R. J., WEINER, R. A., LAROUERE, E., AND STANUTZ, R. N., In-Reactor Corrosion Performance of ZIRLO and Zircaloy-4, Zirconium in the Nuclear Industry: 10th International Symposium, ASTM STP1245, ASTM, Philadelphia (1994) 724–744, https://doi.org/10.1520/STP1245-EB.
- [5] STELLWAG, B., The mechanism of oxide film formation on austenitic stainless steels in high temperature water, Corrosion Science 40 2-3 (1998) 337–370, https://doi.org/10.1016/S0010-938X(97)00140-6.
- [6] LISTER, D. H., DAVIDSON, R. D., McALPINE, E., The mechanism and kinetics of corrosion product release from Stainless Steel in lithiated high temperature water, Corrosion Science 27 2 (1987) 113–1411, https://doi.org/10.1016/0010-938X(87)90068-0.